Available online at www.sciencedirect.com
SCIENCE DIRECT
International Journal of Fatigue 27 (2005) 1398–1407
International Journal of Fatigue
www.elsevier.com/locate/ijfatigue

Crack retardation equations for the propagation of branched fatigue cracks

M.A. Meggiolaro[a,*], A.C.O. Miranda[b], J.T.P. Castro[a], L.F. Martha[c]

[a]Department of Mechanical Engineering, Pontifical Catholic University of Rio de Janeiro, Rua Marquês de São Vicente 225—Gávea, Rio de Janeiro, RJ 22453-900, Brazil
[b]Tecgraf—Computer Graphics Technology Group, Pontifical Catholic University of Rio de Janeiro, Rua Marquês de São Vicente 225—Gávea, Rio de Janeiro, RJ 22453-900, Brazil
[c]Department of Civil Engineering, Pontifical Catholic University of Rio de Janeiro, Rua Marquês de São Vicente 225—Gávea, Rio de Janeiro, RJ 22453-900, Brazil

Available online 30 August 2005

Abstract

The stress intensity factors (SIF) associated with branched fatigue cracks can be considerably smaller than that of a straight crack with the same projected length, causing crack growth retardation or even arrest. This crack branching mechanism can quantitatively explain retardation effects even when plasticity induced crack closure cannot be applied, e.g. in high R-ratio or in some plane strain controlled fatigue crack growth problems. Analytical solutions have been obtained for the SIF of branched cracks, however, numerical methods such as Finite Elements (FE) or Boundary Elements (BE) are the only means to predict the subsequent curved propagation behavior. In this work, a FE program is developed to calculate the path and associated SIF of branched cracks, validated through experiments on 4340 steel ESE(T) specimens. From these results, semi-empirical crack retardation equations are proposed to model the retardation factor along the crack path. The model also considers the possible interaction between crack branching and other retardation mechanisms.

Keywords: Crack retardation model; Bifurcated cracks; Finite elements; Life prediction

1. Introduction

Fatigue cracks can significantly deviate from their Mode I growth direction due to the influence of overloads, multiaxial stresses, micro structural inhomogeneities (such as inclusions, grain boundaries and interfaces), or environmental effects, generating crack kinking or branching [1]. A fatigue crack deviated from its nominal Mode I plane induces mixed-mode near-tip conditions even if the far-field stress is pure traction. For instance, a pure Mode I stress intensity factor (SIF) K_I locally induces Modes I and II SIF k_1 and k_2 near the longer branch b of a bifurcated crack and k_1' and k_2' near the shorter c one. The equivalent SIF K_b and K_c of the longer and shorter branches, calculated respectively from (k_1, k_2) and (k_1', k_2') using e.g. the $\sigma_{\theta\max}$ criterion [2], can be considerably smaller than that of a straight crack with the same projected (on the original crack plane) length, see Fig. 1. Therefore, such branching can retard or even arrest subsequent crack growth [3].

It is experimentally observed that very small differences between the crack branch lengths b and c are enough to cause the shorter branch c to arrest while the larger one b propagates, generally changing its curvature at a retarded rate until returning approximately to its pre-overload SIF and growth direction and rate, see Fig. 1. Therefore, although many branches can be developed along the main crack path, only the fastest branch continues to grow, while all others are brought to a stop due to a shielding effect. This typical propagation behavior has been observed in many structural components, e.g. on a branched crack on an aircraft wheel rim made of 2014-T6 aluminum alloy [4].

Some analytical solutions have been obtained for the SIF of kinked and branched cracks, but it is generally recognized that it is very difficult to develop accurate analytical solutions to their complex propagation behavior [5–9]. Therefore, numerical methods such as Finite Elements (FE) and Boundary Elements (BE) are the only practical means to predict the propagation behavior of branched cracks [10].

* Corresponding author. Tel.: +55 21 3114 1638; fax: +55 21 3114 1165.
E-mail addresses: meggi@mec.puc-rio.br (M.A. Meggiolaro), amiranda@tecgraf.puc-rio.br (A.C.O. Miranda), jtcastro@mec.puc-rio.br (J.T.P. Castro), lfm@civ.puc-rio.br (L.F. Martha).

0142-1123/$ - see front matter © 2005 Elsevier Ltd. All rights reserved.
doi:10.1016/j.ijfatigue.2005.07.016

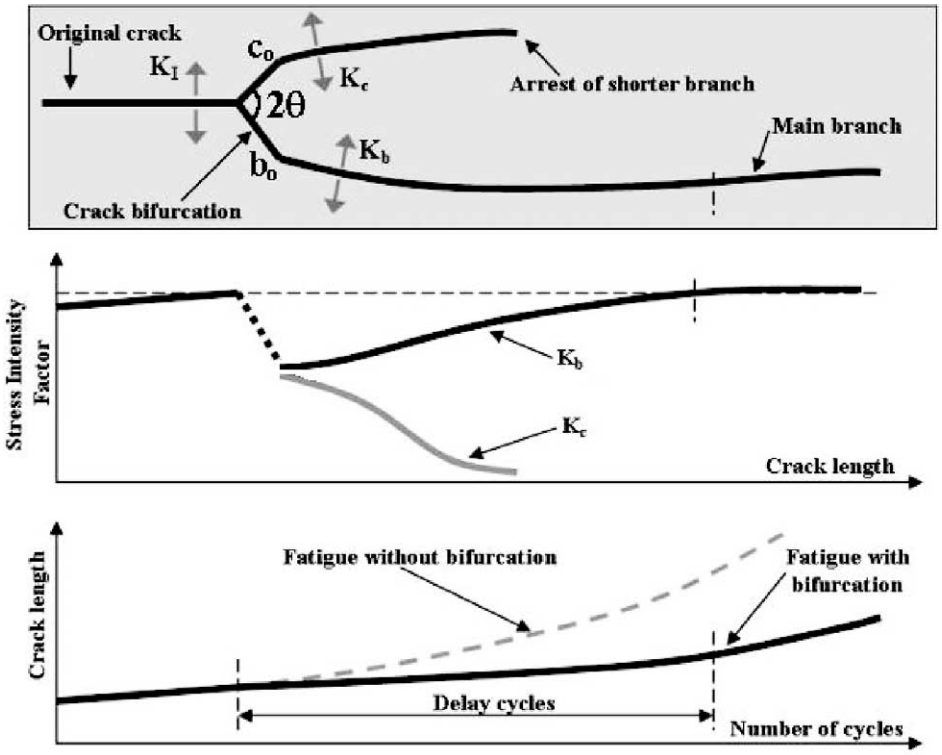

Fig. 1. Bifurcated crack propagation behavior.

A summary of such SIF solutions as a function of the deflection angle and the length of the deflected part of the crack is presented in [11].

To predict the (generally curved) path of a branched crack and to calculate the associated Modes I and II SIF, a specially developed interactive FE program named Quebra (meaning fracture in Portuguese) is used [12]. This program simulates 2D fracture processes based on a FE self-adaptive strategy, using appropriate crack tip elements and crack increment criteria. The adaptive FE analyses are coupled with modern and very efficient automatic remeshing schemes. An efficient meshing algorithm is fundamental to avoid elements with poor aspect ratio and numerical instabilities, since the ratio between the size of the larger and smaller elements can be above 1000 in crack bifurcation calculations. To accomplish that, Quebra uses an innovative algorithm incorporating a quadtree procedure to develop local guidelines to generate elements with the best possible shape. The internal nodes are generated simultaneously with the elements, using the quadtree procedure only as a node-spacing function. This approach tends to give a better control over the generated mesh quality and to decrease the amount of heuristic cleaning-up procedures. Moreover, it specifically handles discontinuities in the domain or boundary of the model. Finally, to enhance the mesh element shape quality, an *a posteriori* local mesh improvement procedure is used [13]. The crack propagation calculations are described in the next section.

2. Propagation of branched cracks

The growth of branched cracks is studied using the Quebra program to model a $C(T)$ specimen with width $w=32.0$ mm, crack length $a=14.9$ mm, and a very small bifurcation with angle 2θ ranging from 40 to 168°, initial longer branch length $b_0=10$ μm and initial shorter branch lengths ranging from $c_0=5$ to 10 μm. A fixed crack growth step of $\Delta b=3$ μm (or 1 μm during the first propagation steps) is considered for the propagation of the longer branch b. This growth step is calculated in the direction defined by the $\sigma_{\theta\max}$ criterion [2]. Due to the differences in the SIF and crack growth rate, a growth step Δc smaller than Δb is expected for the shorter branch. This smaller step is obtained assuming a crack propagation law that models the first two growth phases

$$\frac{da}{dN} = A \times [\Delta K - \Delta K_{th}(R)]^m \tag{1}$$

where A and m are material constants and $\Delta K_{th}(R)$ is the fatigue crack propagation threshold at the $R=K_{min}/K_{max}$ ratio of the test. If ΔK_b and ΔK_c are, respectively, the stress intensity ranges of the longer and shorter branches, then the growth step Δc of the shorter branch c should be

$$\Delta c = \Delta b \left(\frac{\Delta K_c - \Delta K_{th}(R)}{\Delta K_b - \Delta K_{th}(R)} \right)^m \tag{2}$$

Interestingly, the ratio between the propagation rates of the two branches is independent of the material constant A.

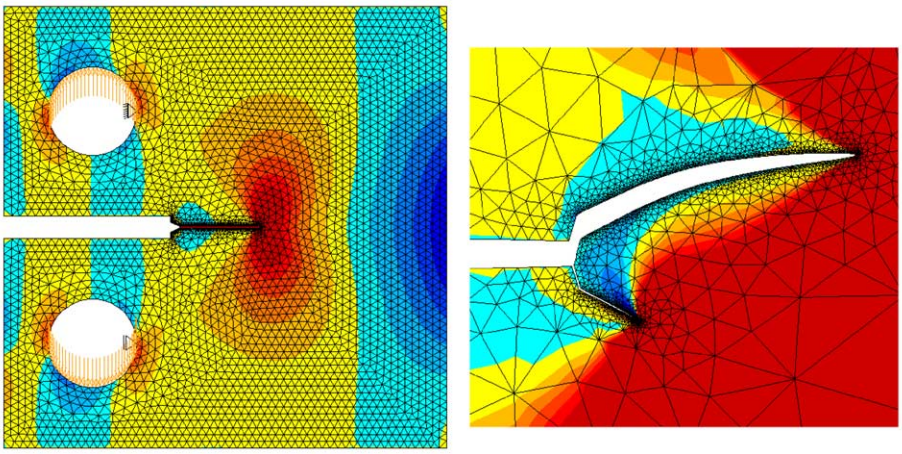

Fig. 2. Propagation simulation of a bifurcated crack on a C(T) specimen (left), and close-up view of the two original 11 and 10 μm branches with angle $2\theta = 150°$ (right).

In this analysis, the exponent m is assumed to be 2.0, 3.0, and 4.0, which are representative for the range of the measured exponents for structural alloys. A similar expression can be obtained if other crack retardation mechanisms are considered, through Lang and Marci's propagation threshold K_{PR} [14] with A and m parameters fitted for each considered load ratio R

$$\Delta c = \Delta b \left(\frac{K_{\max,c} - K_{PR}}{K_{\max,b} - K_{PR}} \right)^m \tag{3}$$

where $K_{\max,b}$ and $K_{\max,c}$ are the maximum SIF of the longer and shorter branches, respectively. Or this threshold K_{PR} can be replaced by the limiting value $K^*_{\max}$ or the threshold of the maximum of Sadananda and Vasudevan's Unified Approach [15,16], which assumes that a crack can propagate only when $\Delta K > \Delta K^*_{th}$ and $K_{\max} > K^*_{\max}$, where $\Delta K^*_{th} = \Delta K_{th}(R \to 1)$.

Both the crack path and the associated SIF along each branch are obtained using the Quebra program. Several calculations were performed for different values of the exponent m, bifurcation angle 2θ, relation c_0/b_0, and SIF, considering or not the effect of K_{PR}, as described next.

2.1. Branched crack propagation with $K_{PR} = 0$

In this section, the propagation behavior of branched cracks is studied using FE but neglecting any retardation mechanism other than the bifurcation itself (i.e. assuming $K_{PR} = 0$). Fig. 2 shows the contour plots of the normal stress component in the load direction axis and propagation results for a bifurcated crack with angle $2\theta = 150°$, obtained from the FE analysis for $c_0/b_0 = 0.91$, $m = 2$ and no closure. In this figure, the deformations are highly amplified to better visualize the crack path. Note that the crack path deviates from the original branch angles, deflecting from ± 75 to approximately $\pm 28°$. In addition, the originally shorter branch arrests after propagating (only) about 29 μm, while the longer branch returns to the pre-overload growth direction and SIF (even though the subsequent crack growth plane may be offset from the pre-overload one, see Fig. 2).

Fig. 3 shows the crack paths obtained from the FE analyses of bifurcated cracks with $2\theta = 130°$ and $c_0/b_0 = \{0.5, 0.8, 0.95, 1\}$, considering $m = 2$ and $K_{PR} = 0$. The dashed lines show the theoretical propagation behavior of a perfectly symmetric bifurcation ($c_0/b_0 = 1$). In this case, the retardation effect would never end because both branches would propagate symmetrically without arresting. Clearly, such behavior is not observed in practice, since the slightest difference between b_0 and c_0 would be sufficient to induce an asymmetrical behavior. Fig. 3 also shows that lower c_0/b_0 ratios result in premature arrest of the shorter crack branch, leading to smaller retardation zones. Also, the propagation path of the longer branch is usually restrained to the region within the dashed lines, while the shorter one is 'pushed' outside that envelope due to shielding effects.

The size of the retardation zone can be estimated from the ratio b_f/b_0, where b_f is the value of the length parameter b of the longer branch (measured along the crack path) beyond which the retardation effect ends. The ratio b_f/b_0 is then calculated through FE propagation simulations for all

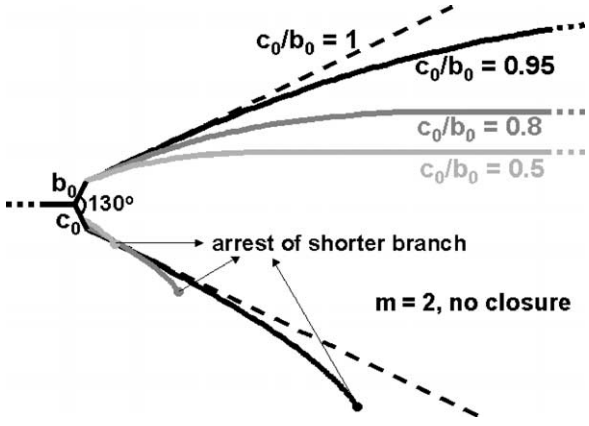

Fig. 3. Bifurcated crack paths for several c_0/b_0 ratios ($K_{PR} = 0$).

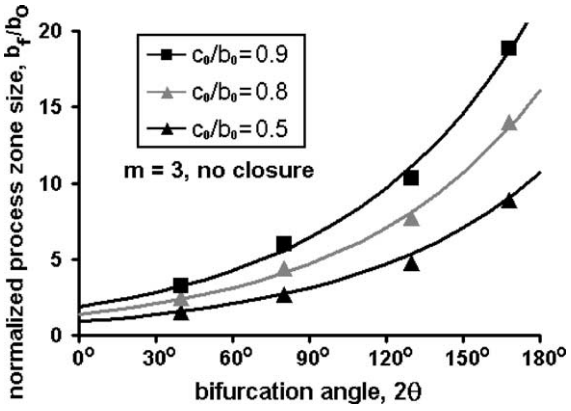

Fig. 4. Normalized process zone size as a function of the bifurcation angle and branch asymmetry c_0/b_0 ($m=3$, $K_{PR}=0$).

combinations of $c_0/b_0=\{0.5, 0.8, 0.9, 0.95\}$, $2\theta=\{40,80, 130,168^\circ\}$ and $m=\{2,3,4\}$, and fitted by the proposed empirical function:

$$\frac{b_f}{b_0}=\exp\left(\frac{2\theta-30^\circ}{56+17(m-2)^{2/3}}\right)/(1-c_0/b_0)^{(12-m)/20} \quad (4)$$

Fig. 4 shows a comparison between the fitted and the FE-obtained data. Note that a greater symmetry between the branches (as c_0/b_0 approaches 1.0) results in a longer retardation zone, as expected from the delayed arrest of the shorter branch.

The FE-calculated equivalent SIF K_b and K_c of the longer and shorter branches are now evaluated along the obtained crack paths. Fig. 5 plots the crack retardation factors (defined as the ratios between K_b or K_c and the Mode I SIF K_I of a straight crack) for $2\theta=130^\circ$ and $m=2$, as a function of the normalized length $(b-b_0)/b_0$ of the longer branch. Because of the different crack branch lengths, the SIF at the longer one is much higher than that at the shorter branch. Assuming K_b and K_c to be the crack driving force, it can be seen from Fig. 5 that the longer branch reaches its minimum propagation rate right after the bifurcation occurs, returning to its pre-overload rate as the crack tip advances away from the influence of the shorter branch. As seen in the figure, the retardation behavior is misleadingly similar to closure-related effects, even though no closure is present in that case.

In addition, as the length difference between both branches increases, it is expected that the propagation rate of the shorter one is reduced until it arrests, after which the larger branch will dominate. Note that even small differences between the branch lengths, such as in the case $c_0/b_0=0.95$ shown in Fig. 5, are sufficient to cause subsequent arrest of the shorter branch.

An empirical expression is here proposed to model the SIF K_b of the longer branch during the transition between K_{b0} (the value of K_b immediately after the bifurcation event) and the straight-crack K_I (after the retardation effect ends), valid for $b_0\le b\le b_f$ and $0.7<c_0/b_0<1$

$$K_b=K_{b_0}+(K_I-K_{b_0})\left[a\tan\left(3\frac{b-b_0}{b_f-b_0}\right)/1.25\right]^{2c_0/b_0} \quad (5)$$

where b_f is given in Equation (4) and K_{b0} (and K_{c0}) by

$$\frac{K_{b0}}{K_I}=0.75+(1-\sin\theta)\left(1-\frac{c_0}{b_0}\right),\qquad \frac{K_{c0}}{K_I}=0.75-(1-\sin\theta)\left(1-\frac{c_0}{b_0}\right) \quad (6)$$

It must be pointed out, however, that the presented FE results and empirical models might have some limitations, because actual bifurcations can be of a size comparable to the scale of the local plasticity (e.g. of the plastic zone size) or microstructural features (e.g. of the grain size). Moreover, possible environmental effects should be considered when comparing the bifurcation model predictions with measured crack growth rates [3]. However, one could argue that similar limitations would also apply to straight and in particular to curved crack propagation problems, since the crack increments (which are of the order of the CTOD, or of K^2/ES_Y, where E is Young's modulus and S_Y the yield strength) are at least two orders of magnitude smaller than the scale of the local plasticity (which is proportional to $(K/S_Y)^2$) in all these cases. But nevertheless 2D LEFM

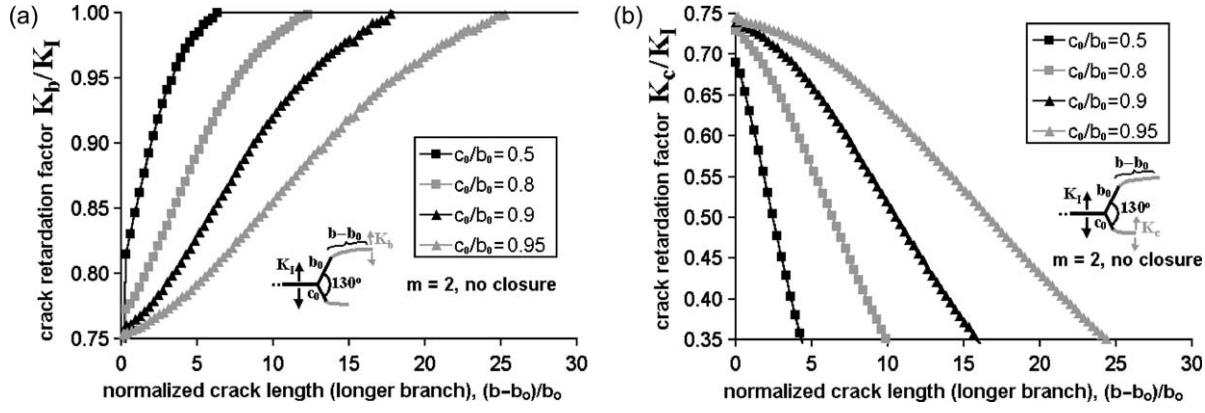

Fig. 5. Normalized equivalent SIF for the (a) longer and (b) shorter branch of a bifurcated crack during its propagation ($2\theta=130^\circ$, $m=2$, $K_{PR}=0$).

concepts are highly successful in modeling those problems when the local plasticity is much smaller than cracked piece dimensions [12,13]. In other words, experience has validated the use of a global SIF elastic parameter to predict the direction and the amount of the local crack increment, which is much smaller than the size of the plastic zones that always accompany the crack tip. Using these same concepts to describe the path and propagation life of a bifurcated crack under similar small scale yielding conditions (but not to describe how it bifurcates after an overload, e.g.) thus seems a very reasonable initial modeling approach for such problems (pending, of course, support by proper experimental verification). The interaction between crack branching and other retardation mechanisms is studied next.

2.2. Influence of other mechanisms on branched crack propagation

All presented branched growth simulations so far have not included the effect of other retardation mechanisms. This effect is easily accounted for in the FE calculations using Eq. (3). The limiting value K_{PR} is assumed to be the same at both branch tips and always larger than the minimum SIF of each branch. Further simulations are then conducted considering several K_{PR} values, normalized by the maximum Mode I SIF K_I of the straight crack, namely $K_{PR}/K_I = \{0.067,0.08,0.10,0.13,0.20,0.25,0.40,0.57\}$.

A generalized version of Eq. (4) is then proposed to fit the calculated process zone sizes including the combined effects of other mechanisms:

$$\frac{b_f}{b_o} = \frac{\alpha}{(1-c_0/b_0)^{(12-m)/20}} \times \exp\left[\frac{-\beta}{(1-c_0/b_0)^{\gamma}} \frac{K_{PR}}{K_I}\right] \tag{7}$$

where

$$\alpha = \exp\left(\frac{2\theta - 30^\circ}{56 + 17(m-2)^{2/3}}\right) \tag{8}$$

$$\beta = \left(\frac{2\theta}{110 + 60(m-2)^{0.6}}\right)^{5/2} \tag{9}$$

$$\gamma = \frac{180^\circ - 2\theta}{280 - 130(m-2)^{0.3}} \tag{10}$$

Note that the ratio K_{PR}/K_I in Eq. (7) should be replaced with zero if K_{PR} is smaller than the minimum SIF of both branches. Figs. 6 and 7 show a comparison between the fitted and the FE-obtained data as a function of the ratio K_{PR}/K_I. Note that greater K_{PR} levels result in shorter retardation zones, because the shorter branch is more easily arrested due to the reduction in its stress intensity range.

Fig. 8 shows the effect of K_{PR} at the branch tips on the retardation factor for $2\theta = 130^\circ$, $c_0/b_0 = 0.9$ and $m = 2$. Note that higher K_{PR} levels reduce the size of the retardation process zone, due to premature arrest of the shorter branch. In Fig. 8, e.g. the normalized size of the process zone is

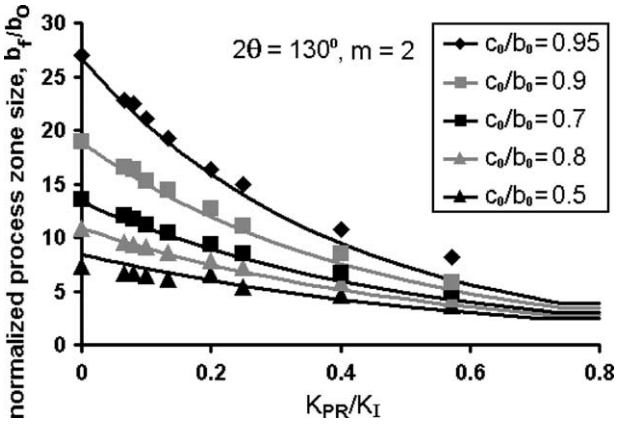

Fig. 6. Normalized process zone size of bifurcated cracks as a function of K_{PR} and branch asymmetry c_0/b_0 ($2\theta = 130^\circ$, $m = 3$).

reduced from 18 to 3.6 as K_{PR}/K_I approaches 0.74, a factor of 5. In this example, 0.74 is the minimum K_{PR}/K_I level that prevents the shorter branch to even start propagating. Therefore, at any level above 0.74 the normalized process zone size will also be 3.6, because the propagation geometry will remain unchanged as long as the shorter branch remains arrested at $c = c_0$.

Note, however, that a smaller process zone does not necessarily mean fewer delay cycles, since the longer branch will also experience a reduction in the crack propagation rate due to other retardation mechanisms. Therefore, a competition between lower growth rates of the longer branch and smaller bifurcation process zone sizes will take place to determine the real effect of combining bifurcation with other retardation mechanisms.

Eqs. (7)–(10) and (6) can then be applied to Eq. (5) to model the SIF K_b of the longer branch during the transition between K_{b0} (the SIF immediately after the bifurcation event) and the straight-crack K_I (the SIF after the end of the retardation effect), completing this analysis.

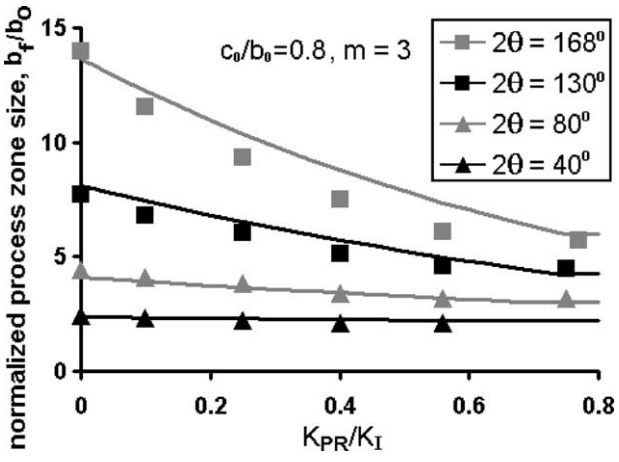

Fig. 7. Normalized process zone size of bifurcated cracks as a function of K_{PR} and bifurcation angle 2θ ($c_0/b_0 = 0.8$, $m = 3$).

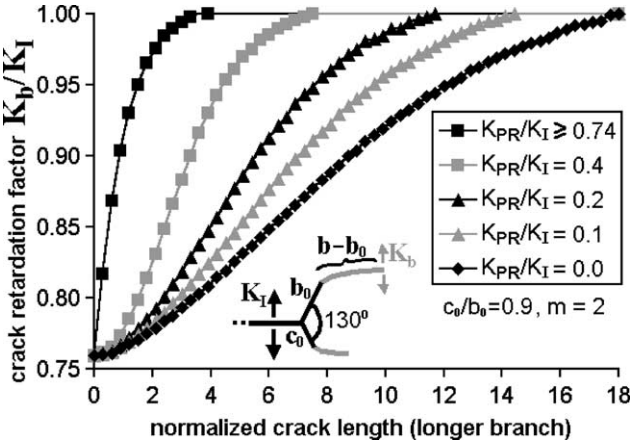

Fig. 8. Normalized SIF of the longer branch during its propagation as a function of the normalized length $(b-b_0)/b_0$ for several K_{PR} levels ($c_0/b_0=0.9$, $m=2$).

3. Experimental results

Quantitative validations of the predicted bifurcated crack growth behavior are performed on Eccentrically-loaded Single Edge Crack Tension specimens ESE(T) made from an annealed SAE 4340 alloy steel with $S_Y=377$ MPa, $S_U=660$ MPa, $E=205$ GPa, and RA = 52.7%, and with the analyzed weight percent composition: C 0.37, Mn 0.56, Si 0.14, Ni 1.53, Cr 0.64, Mo 0.18, S 0.04, P 0.035. The tests are performed at frequencies between 20 and 30 Hz in a 250 kN computer-controlled servo-hydraulic testing machine. The crack length is measured following ASTM E 647 procedures [17]. Special attention is given for crack closure measurements, made using a high-speed data acquisition system to obtain data and to avoid intervention during the tests. In this way, the load and Crack-Opening Displacement (COD) data are used to precisely compute the crack closure load using a digital implementation of the linearity subtractor circuit developed to enhance the opening load, [18] (the accuracy of such careful closure load measurements is in the order of $K_{max}/100$ [19]).

The proposed retardation equations are implemented in a fatigue life assessment program named ViDa [12–13]. This program is used to estimate the number of delay cycles associated with the experimentally obtained bifurcation on the 4340 steel ESE(T) specimen. The number of cycles spent during the propagation in the retardation region is then calculated by integrating the da/dN equation along the longer crack branch, from $b=b_0$ to $b=b_f$.

Four tests are performed on ESE(T) specimens subject to 100% overloads, namely tests I, II, III and IV: (I) $R=0.7$, $\Delta K=13.9$ MPa$\sqrt{\text{m}}$, resulting in approximately 22,000 delay cycles; (II) $R=0.7$, $\Delta K=14.2$ MPa$\sqrt{\text{m}}$, resulting in approximately 20,000 delay cycles; (III) $R=0.7$, $\Delta K=13.7$ MPa$\sqrt{\text{m}}$, resulting in approximately 27,000 delay cycles; (IV) $R=0.05$, $\Delta K=16.2$ MPa$\sqrt{\text{m}}$, resulting in approximately 32,000 delay cycles, see Figs. 9–18.

It is found that the minimum load levels in tests I and II are always above the opening load, therefore, no crack closure is present nor before nor after the overloads. For test I, the measured initial branch lengths are approximately $b_0=9$ μm and $c_0=8.5$ μm, with a bifurcation angle $2\theta=160°$, see Fig. 9(a). The material is modeled using Eq. (1) with crack growth constants $A=9\times10^{-11}$ m/cycle and $m=2.1$, and a propagation threshold $\Delta K_{th}=2.8$ MPa$\sqrt{\text{m}}$, measured under $R=0.7$. From Eq. (6), it is found that $K_{b0}/K_I=0.751$ and $K_{c0}/K_I=0.749$, leading to $\Delta K_{b0}=0.751\ \Delta K_I=10.437$ MPa$\sqrt{\text{m}}$ and $\Delta K_{c0}=0.749\ \Delta K_I=10.413$ MPa$\sqrt{\text{m}}$. Since both ranges are greater than $\Delta K_{th}(R=0.7)=2.8$ MPa$\sqrt{\text{m}}$, both branches are expected to start propagating, as verified experimentally. The size of the process zone can be estimated from Eq. (4), which results in $b_f=36.95\times9$ μm $\cong 332$ μm. The number of delay cycles n_D is then calculated by:

$$n_D = \int_{b_0}^{b_f} \frac{db}{A(\Delta K_b - \Delta K_{th})^m} - \int_{b_0}^{b_f} \frac{db}{A(\Delta K_I - \Delta K_{th})^m}$$
$$= \int_{9}^{332} \frac{db\times10^{-6}}{9\cdot10^{-11}\left\{7.64+2.27\left[a\tan\left(3\frac{b-9}{332-9}\right)/1.25\right]^{1.88}\right\}^{2.1}}$$
$$- \int_{9}^{332} \frac{db\times10^{-6}}{9\cdot10^{-11}(13.9-3.8)^{2.1}} = 9,664 \text{ cycles} \qquad (11)$$

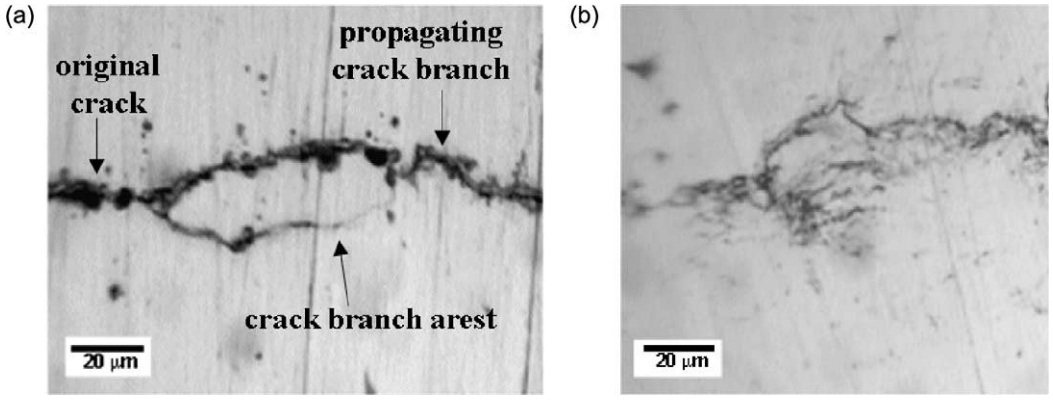

Fig. 9. Crack bifurcation experiments on SAE 4340 steel: (a) test I, (b) test II.

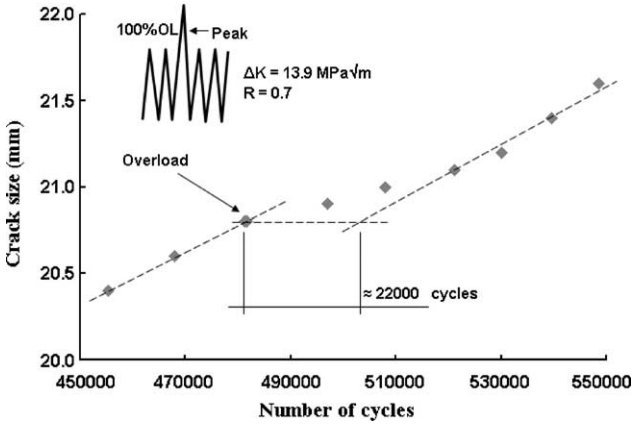

Fig. 10. Fatigue crack growth retardation after a 100% overload, $R=0.7$ (test I).

which is approximately half of the measured 22,000 delay cycles (Fig. 10).

For test II, the measured initial branch lengths are approximately $b_0=10$ μm and $c_0=9.5$ μm, but with a larger bifurcation angle $2\theta=160°$, see Fig. 9(b), resulting in:

$$n_D = \int_{b_0}^{b_f} \frac{db}{A(\Delta K_b - \Delta K_{th})^m} - \int_{b_0}^{b_f} \frac{db}{A(\Delta K_I - \Delta K_{th})^m}$$

$$= 36,093 - 25,424 = 10,669 \quad (12)$$

which is also about half of the measured 20,000 delay cycles (Fig. 11).

Fig. 12 shows a crack retardation of approximately 22,000 delay cycles resulting from test III. However, in this case the external polished surfaces of the specimen did not present any signs of bifurcation. But careful inspection of the fracture surfaces using a scanning electron microscope revealed that not only tests I and II but also test III resulted in a bifurcation front along the specimen thickness, see Figs. 13–15. The bifurcation front is approximately straight and through-the-thickness for tests I and II, but surprisingly

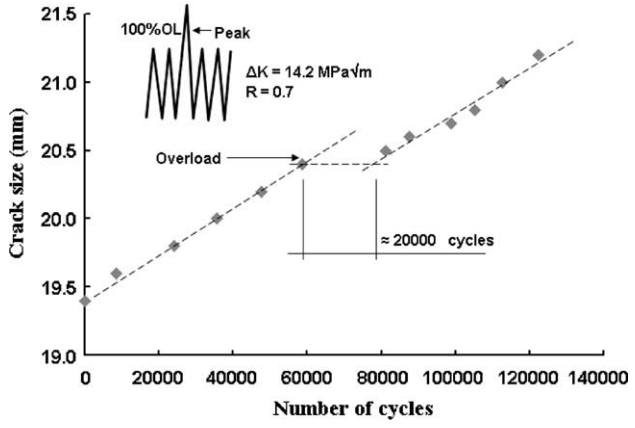

Fig. 11. Fatigue crack growth retardation after a 100% overload, $R=0.7$ (test II).

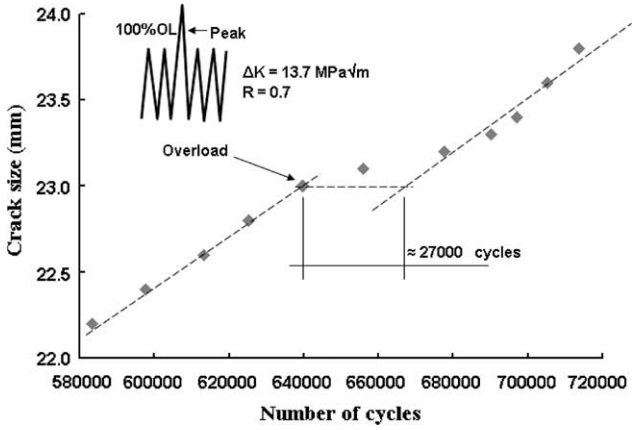

Fig. 12. Fatigue crack growth retardation after a 100% overload, $R=0.7$ (test III).

for test III the front is discontinuous towards the specimen faces, indicating an internal bifurcation. Despite its 3D geometry, the retardation behavior is still reasonably reproduced by the proposed 2D model within a factor of 2 in number of delay cycles.

For test IV, the initial branch lengths are approximately $b_0=10$ and $c_0=9.5$ μm, with a bifurcation angle $2\theta=150°$, see Fig. 16. The material is modeled using Eq. (1) with crack growth constants $A=9\times10^{-11}$ m/cycle and $m=2.2$, and a propagation threshold $\Delta K_{th}=8.1$ MPa$\sqrt{\text{m}}$, all measured under $R=0.05$. The size of the process zone is calculated from Eqs. (7–10), resulting in $\alpha=6.97$, $\beta=1.35$, $\gamma=0.15$, and $b_f=11.6\times10$ μm $\cong 116$ μm. Using the same process described previously, the delay cycles n_D is estimated by:

$$n_D = \int_{b_0}^{b_f} \frac{db}{A(\Delta K_b - \Delta K_{th})^m} - \int_{b_0}^{b_f} \frac{db}{A(\Delta K_I - \Delta K_{th})^m}$$

$$= 33,961 - 16,645 = 17316 \quad (13)$$

which is about half of the measured 32,000 delay cycles, see Fig. 17.

Note that in all tests there was no retardation induced by crack closure. The only test in which crack closure was detected was test IV, however after the overload the opening load in fact decreased, see Fig. 18. The opening load remained lower than before the overload along the entire process zone, only returning to its original value after the bifurcation effect had ended. Therefore, even if closure affected the constant amplitude growth behavior in test IV, it would not be able to explain the measured overload-induced retardation. This behavior has already been described in the literature [20].

The errors in the predictions performed using the proposed semi-empirical equations can be explained by inaccuracies in the estimation of the initial branch lengths b_0 and c_0, since the retardation effect is highly dependent on the ratio c_0/b_0. In addition, other retardation mechanisms

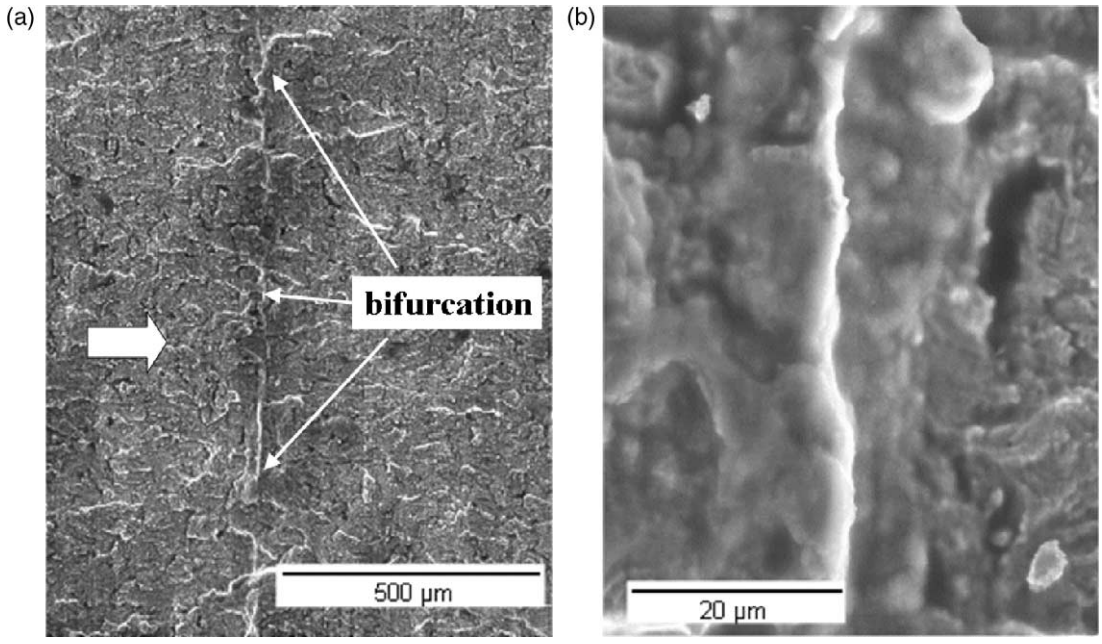

Fig. 13. Scanning electron micrographs of fracture surfaces (test I): (a) bifurcation front through the specimen thickness, and (b) detailed view indicating different height levels.

besides bifurcation (except for closure, as discussed above) might be contributing to increase the number of delay cycles, such as unmodeled environmental effects or further kinking of the branch tips due to microstructure inhomogeneities. Another factor could be a specimen thickness effect, where the plane strain condition assumed in the 2D calculations would result in less retardation than the actual 3D stress state. However, the retardation mechanism behind a possible thickness effect in the performed experiments could not be crack closure, as shown in Fig. 18. Small differences between the actual crack growth behavior and the assumed crack propagation rule (particularly in the curvature of the transition from the threshold or phase I to the Paris or phase II regions) can also be a cause for these prediction inaccuracies. In any case, the presented predictions are of the same order of magnitude of the experimental scatter. Therefore, the quantitative approach presented in this work is a quite promising tool for modeling and

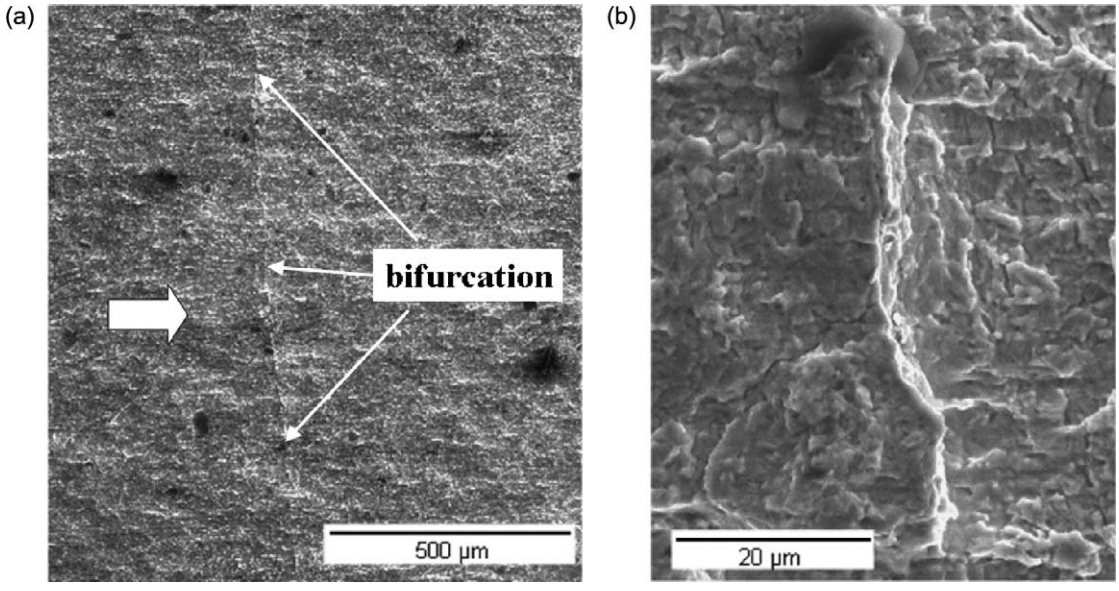

Fig. 14. Scanning electron micrographs of fracture surfaces (test II): (a) bifurcation front through the specimen thickness, and (b) detailed view indicating different height levels.

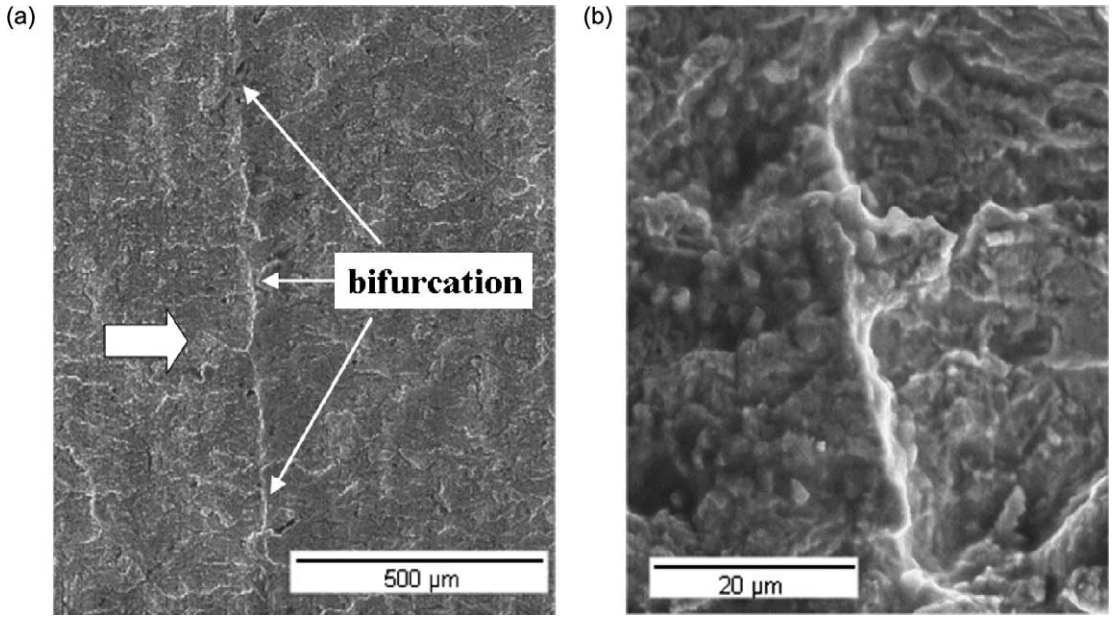

Fig. 15. Scanning electron micrographs of fracture surfaces (test III): (a) bifurcation front through the specimen thickness, and (b) detailed view indicating different height levels.

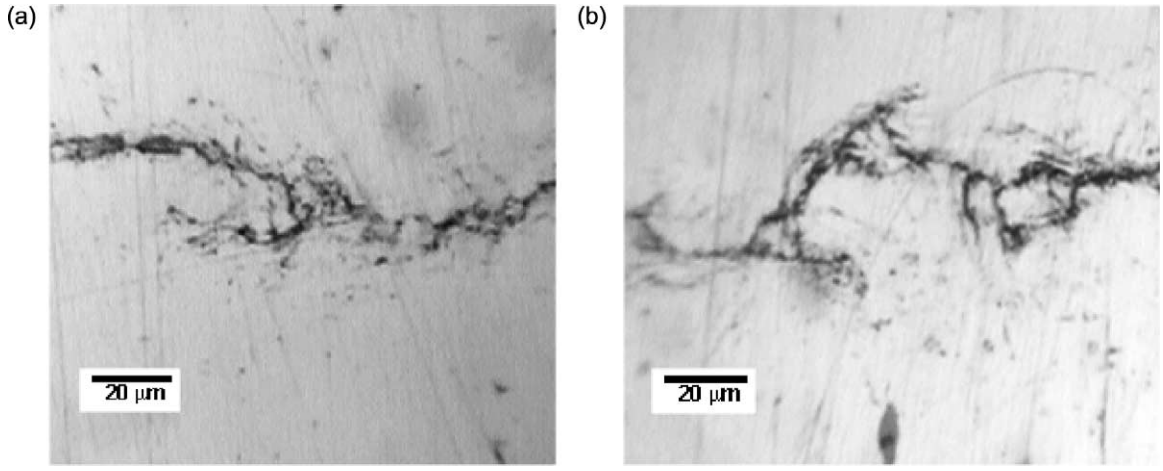

Fig. 16. Crack bifurcation experiments on SAE 4340 steel (test IV): (a) front face of specimen (b) back face of specimen.

calculating overload-induced retardation effects where other mechanisms have failed to give a satisfactory explanation.

Finally, it must be noted as well that all measured bifurcations occurred throughout the thickness in an approximately uniform pattern (except near the specimen faces for test III), observed after carefully slicing and reexamining the specimens. Therefore, despite the inherent 3D nature of the bifurcation problem, in these tests the presented 2D FE approach has been validated.

4. Conclusions

In this work, a specialized FE program was used to calculate the propagation path and associated stress intensity factors (SIF) of bifurcated cracks, which can

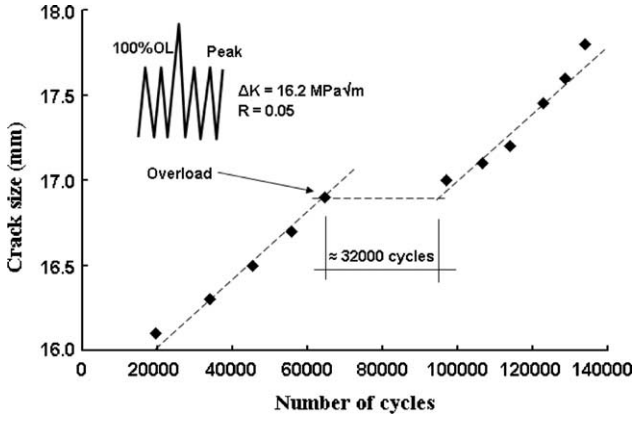

Fig. 17. Fatigue crack growth retardation after a 100% overload, $R=0.05$ (test IV).

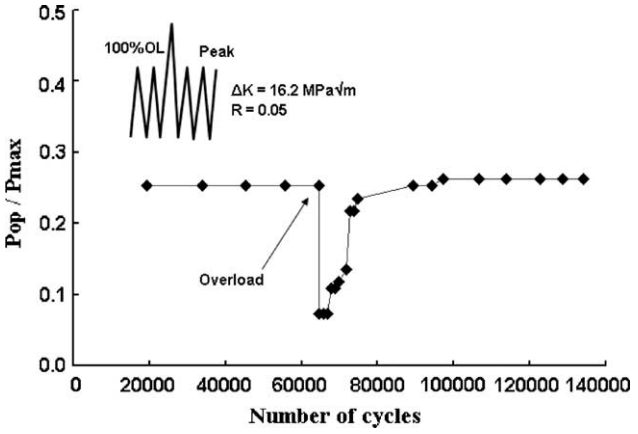

Fig. 18. Opening load measurements, before and after the overload (test IV)
.

cause crack retardation or even arrest. A total of 262 crack propagation simulations were obtained from a total of 6250 FE calculation steps to fit empirical equations to the process zone size and crack retardation factor along the curved crack branches. In particular, the bifurcation simulations included several combinations of bifurcation angles $2\theta = \{40, 80, 90, 130, 168°\}$, branch asymmetry ratios $c_0/b_0 = \{0.5,0.7,0.8, 0.9,0.95,1.0\}$, crack growth exponents $m = \{2,3,4\}$, and even considered interaction between crack branching and other retardation mechanisms through the threshold ratios $K_{PR}/K_I = \{0.0,0.067,0.08,0.10,0.13,0.20,0.25,0.40,0.57\}$. It was shown that very small differences between the lengths of the bifurcated branches are sufficient to cause the shorter one to eventually arrest as the longer branch returns to the pre-overload conditions. The process zone size was found to be smaller for lower bifurcation angles and for branches with greater asymmetry, in both cases due to the increased shielding effects on the shorter branch. The retardation zone was reduced as well for materials with higher crack growth exponents, due to the increased difference between the crack growth rates of the longer and shorter branches. Higher K_{PR} levels also resulted in smaller process zones, because the shorter branch was more easily arrested due to the reduction in its stress intensity range. However, a competition between smaller process zone sizes and lower growth rates of the longer branch did take place to determine the real effect of combined bifurcation and other retardation mechanisms. The proposed equations, besides capturing all above described phenomena, can be readily used to predict the propagation behavior of branched and kinked cracks in an arbitrary structure, as long as the process zone ahead of the crack tip is small compared to the other characteristic dimensions, exactly as in other similar fatigue propagation problems such as curved crack path and life predictions. However, these predictions probably should also be limited to the cases where it can be assumed that the entire crack-front bifurcates uniformly (as observed byscanning electron microscopy in the tests reported in this work), where the specimen thickness itself may provide the size scale requirements for the validity of the presented 2D LEFM-based equations, as the calculated SIF may be averaged considering the (several) grains present along the thickness. Otherwise, if the crack deflections vary significantly along the thickness, then 3D modeling including Mode III effects should be considered. From these results, it can be seen that crack bifurcation may provide an alternate mechanistic explanation for overload-induced crack retardation on structural components, especially to explain load interaction effects under closure-free conditions.

References

[1] Lankford J, Davidson DL. The effect of Overloads upon fatigue crack tip opening displacement and crack tip opening/closing loads in aluminum alloys. In: Advances in fracture research. NY, USA: Pergamon Press; 1981. p. 899–906.
[2] Erdogan F, Sih GC. On the crack extension in plates under plane loading and transverse shear. J Basic Eng 1963;85:519–27.
[3] Suresh S. Crack deflection: implications for the growth of long and short fatigue cracks. Metall Trans 1983;14a:2375–85.
[4] Kosec B, Kovacic G, Kosec L. Eng Failure Anal 2002;9:603–9.
[5] Karihaloo BL. On crack kinking and curving. Mech Mater 1982;1: 189–201.
[6] Seelig T, Gross D. On the interaction and branching of fast running cracks—a numerical investigation. J Mech Phys Solids 1999;47: 935–52.
[7] Suresh S. Micromechanisms of fatigue crack growth retardation following overloads. Eng Fract Mech 1983;18(3):577–93.
[8] Suresh S. Fatigue of materials. Cambridge University Press; 1998. p. 679.
[9] Melin S. Why do cracks avoid each other? Int J Fract 1983;23:37–45.
[10] Pärletun LG. Determination of the growth of branched cracks by numerical methods. Eng Fract Mech 1979;11:343–58.
[11] Suresh S, Shih CF. Plastic near-tip fields for branched cracks. Int J Fract 1986;30:237–59.
[12] Miranda ACO, Meggiolaro MA, Castro JTP, Martha LF, Bittencourt TN. Fatigue crack propagation under complex loading in arbitrary 2D geometries. ASTM STP 1411 2002;4:120–46.
[13] Miranda ACO, Meggiolaro MA, Castro JTP, Martha LF, Bittencourt TN. Fatigue life and crack path prediction in generic 2D structural components. Eng Fract Mech 2003;70:1259–79.
[14] Lang M, Marci G. The influence of single and multiple overloads on fatigue crack propagation. Fatigue Fract Eng Mater Struct 1999;22: 257–71.
[15] Sadananda K, Vasudevan AK, Holtz RL. Extension of the unified approach to fatigue crack growth to environmental interactions. Int J Fatigue 2001;23:S277–S86.
[16] Sadananda K, Vasudevan AK. Fatigue crack growth mechanisms in steels. Int J Fatigue 2003;25:899–914.
[17] ASTM Standard E 647. Standard Test Method for Measurement of Fatigue Crack Growth Rates. ASTM Standards; 03.01.
[18] Paris P, Hermann L. Int Cong App Mech, Delft, 1976.
[19] Castro JTP. A circuit to measure crack closure. Exp Tech 1993;17(2): 23–5.
[20] Meggiolaro MA, Castro JTP. On the dominant role of crack closure on fatigue crack growth modeling. Int J Fatigue 2003;25(9–11):843–54.